J Mater Sci (2011) 46:4428–4433
DOI 10.1007/s10853-011-5430-y

IIB 2010

Dislocation structures in a $\{\bar{1}104\}/\langle 11\bar{2}0\rangle$ low-angle tilt grain boundary of alumina (α-Al_2O_3)

E. Tochigi · N. Shibata · A. Nakamura · T. Yamamoto · Y. Ikuhara

Received: 31 August 2010 / Accepted: 2 March 2011 / Published online: 12 March 2011

Abstract An alumina (α-Al_2O_3) bicrystal with a $(\bar{1}104)/[11\bar{2}0]$ 2° low-angle tilt grain boundary was fabricated by diffusion bonding at 1500 °C in air, and the grain boundary was observed by transmission electron microscopy (TEM). High-resolution TEM observations revealed that the grain boundary consists of at least two kinds of dislocations. One is a perfect dislocation which has a Burgers vector of $1/3[\bar{1}2\bar{1}0]$. The other is dissociated into two partial dislocations with a stacking fault on the (0001) plane, and each partial dislocation has a $1/6[\bar{1}101]$ edge component. It is suggested from structural considerations that the dissociated-dislocation pair originates from a $\boldsymbol{b} = 1/3[02\bar{2}1]$ perfect dislocation (i.e., $1/3[02\bar{2}1] \rightarrow 1/6[02\bar{2}1] + 1/6[02\bar{2}1]$). This dissociation produces a stacking fault in the anion sublattice. The stacking fault energy is estimated to be roughly 1.3 Jm^{-2} based on the elastic theory. The authors discuss the dislocation structures and the stacking fault formed on the (0001) plane in detail.

E. Tochigi · N. Shibata · T. Yamamoto · Y. Ikuhara (✉)
Institute of Engineering Innovation, The University of Tokyo, 2-11-16, Yayoi, Bunkyo-ku, Tokyo 113-8656, Japan
e-mail: ikuhara@sigma.t.u-tokyo.ac.jp

N. Shibata
PRESTO, JST, 4-1-8, Honcho Kawaguchi, Saitama 332-0021, Japan

A. Nakamura
Department of Intelligent Materials Engineering, Osaka City University, 3-3-138, Sugimoto, Sumiyoshi-ku, Osaka 558-8585, Japan

T. Yamamoto · Y. Ikuhara
Nanostructures Research Laboratory, Japan Fine Ceramics Center, 2-4-1, Mutsuno, Atsuta-ku Nagoya, Aichi 456-8587, Japan

Y. Ikuhara
WPI-AIMR Research Center, Tohoku University, 2-1-1, Katahira, Aoba-ku, Sendai, Miyagi 980-8577, Japan

Introduction

Alumina (α-Al_2O_3) is widely used as a high-temperature structural ceramic. Since the mechanical properties of crystalline materials are strongly related to dislocation behavior, dislocation structures in alumina have been extensively studied by transmission electron microscopy (TEM) [1–16]. Dislocations in this material often dissociate into two or more partial dislocations with stacking faults in between. In order to identify the dissociation structures, it is necessary to analyze the dislocation core structures at atomic level. However, it is extremely difficult to observe the core structure of lattice dislocations introduced by the deformation processes, because dislocations are often at an incline to the observing direction in TEM. Thus, using grain boundary dislocations which have equivalent structures to lattice dislocations is an alternative method to study dislocation core structures [10–12, 14, 15, 17, 18]. A low-angle grain boundary is formed between two grains which have a slight misorientation, up to about 15° [19, 20]. In the grain boundary, dislocations are periodically introduced to accommodate the misorientation. The dislocation structure depends on the grain boundary plane and the rotational axis. Thus, if the authors can arbitrarily control the grain misorientation, the authors may form the same dislocations as those introduced by the deformation processes along the boundary.

Bicrystal experiments have been extensively performed to investigate the grain boundary structures in alumina [10–15]. Using the bicrystal method, the authors can obtain

grain boundaries which have a well-controlled orientation relationship. In alumina, dislocation structures in $\{11\bar{2}0\}/[0001]$ [10], $\{11\bar{2}0\}/\langle 1\bar{1}00\rangle$ [11, 12, 14], and $\{1\bar{1}00\}/\langle 11\bar{2}0\rangle$ [15] low-angle tilt grain boundaries in bicrystals have been reported so far. It was found that each grain boundary basically consisted of a periodic array of dissociated dislocations with a stacking fault in between. Stacking faults often appeared on the grain boundary plane, because each grain boundary plane was selected to coincide with a high-symmetric crystallographic plane. If less symmetric planes are selected as grain boundary planes, several kinds of dislocation structure may be formed to accommodate the misorientation of the boundary, and stacking faults will not necessarily occur on the grain boundary plane. Therefore, it is interesting to investigate which dislocation structures are formed in such grain boundaries.

In this study, it was observed dislocation structures in a $\{\bar{1}104\}/\langle 11\bar{2}0\rangle$ 2° tilt grain boundary by TEM. The authors will discuss the dislocation structures and the stability of the stacking faults formed in the boundary.

Atomic structure of alumina

The crystal structure of α-Al_2O_3 is the corundum type structure (space group: $R\bar{3}c$). The lattice parameters of the hexagonal unit cell are $a = 4.76$ Å and $c = 12.99$ Å ($c/a = 2.73$) [21]. The atomic configuration is schematically described in Fig. 1. The oxygen ions are approximately arranged in hexagonal close packing, and the aluminum ions are occupied in 2/3 of the octahedral interstices of the anion sublattice. The translation vectors $1/3[11\bar{2}0]$, $1/3[\bar{1}101]$, and $1/3[2\bar{2}01]$ are indicated by the arrows of solid line. The vectors $1/3[1\bar{1}00]$ and 1/3[0001], indicated by the arrows of broken line, correspond to translation vectors in the anion sublattice but not in the cation sublattice. The planes $(1\bar{1}02)$ and $(\bar{1}104)$ are indicated by the broken lines. It is noted that the planes $(\bar{1}104)$ and $(1\bar{1}04)$ are not equivalent crystallographic planes because of a threefold symmetry with respect to the hexagonal *c*-axis. The directions $[\bar{1}101]$ and $[2\bar{2}01]$ are parallel to the $(1\bar{1}02)$ and the $(\bar{1}104)$ planes, respectively, and are separated by an angle of 84.16°.

Experimental procedure

A bicrystal with a $(\bar{1}104)/[11\bar{2}0]$ 2° tilt grain boundary was fabricated by bonding two pieces of high-purity alumina single crystal (>99.99%, Shinkosha Co., Ltd.) in air at 1500 °C for 10 h with a cooling rate of 300 °C/h [10–12, 14, 15]. The schematic illustration of the bicrystal is shown in Fig. 2. The size of the bicrystal was 15 × 12 × 12 mm^3.

A sample for TEM observation was prepared by a standard procedure using the ion thinning method. The bicrystal was cut to about 2 × 1.5 × 0.5 mm^3 with $(11\bar{2}0)$ surfaces using a diamond saw. Subsequently, both the surfaces were mechanically ground to a thickness of about 20 μm and then polished to a mirror finish using diamond slurries. The sample was argon-ion milled (~4 kV) to obtain electron transparency. One side of the sample surface was coated with a thin amorphous-carbon film to avoid charging during observation. The grain-boundary structure was observed with two TEMs: a JEM-2010HC (JEOL, Tokyo), operating at 200 kV, for conventional analysis; and a JEM-4010 (JEOL, Tokyo), operating at 400 kV, for high-resolution analysis. The point-to-point resolution of the JEM-4010 is better than 0.16 nm.

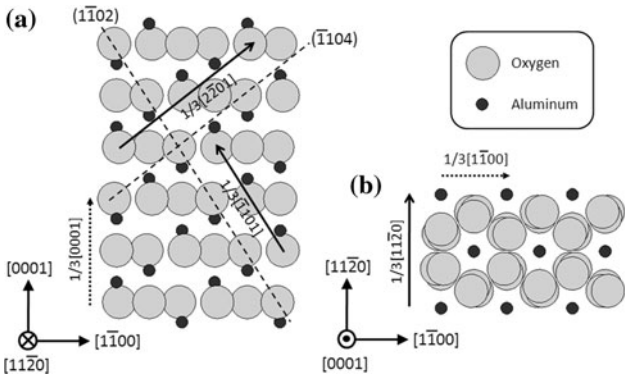

Fig. 1 Schematics showing the crystal structure of alumina viewed from the $[11\bar{2}0]$ and the [0001] directions. The vectors of $1/3[11\bar{2}0]$, $1/3[2\bar{2}01]$, and $1/3[\bar{1}101]$ correspond to translation vectors, which are indicated by the *solid arrows*. The angle between the $(\bar{1}104)$ plane and the $[\bar{1}101]$ direction is 84.76°

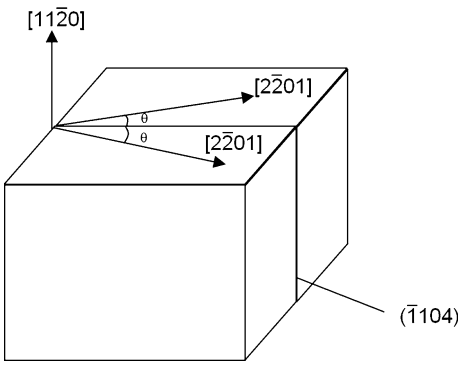

Fig. 2 A schematic of the fabricated alumina bicrystal. The tilt angle 2θ was set to be 2°

Results and discussion

Figure 3 shows a dark-field TEM image of the $(\bar{1}104)$/$[11\bar{2}0]$ grain boundary taken using the reflection $\boldsymbol{g} = (1\bar{1}0\bar{4})$. Small pair contrasts and relatively large contrasts can be seen along the grain boundary. This implies that the grain boundary consists of two or more kinds of dislocations. The periodicity of the contrasts, d, is roughly 15 nm. From the electron diffraction pattern taken from the $[11\bar{2}0]$ zone axis, the tilt angle of the boundary, 2θ, was estimated to be 2.1°. The edge component of the dislocations to accommodate the mistilt, $|\boldsymbol{b}_e|$, can be estimate to be 0.55 nm by Frank's formula [20]:

$$\boldsymbol{b}_e = 2\theta \times d \quad (1)$$

It is reasonable to consider that $\boldsymbol{b}_e$ corresponds to the vector $1/3[\bar{1}101]$ ($|1/3\langle\bar{1}101\rangle| = 0.511$ nm), which is the smallest translation vector along the $[\bar{1}101]$ direction and can efficiently accommodate the misorientation perpendicular to the $(\bar{1}104)$ grain boundary plane.

Since the angle between the $[\bar{1}101]$ direction and the $(\bar{1}104)$ grain boundary plane (or the $[2\bar{2}01]$ direction) is not 90° but rather 84.16°, the vector of $1/3[\bar{1}101]$ will accompany shear of the boundary toward the $[2\bar{2}01]$ direction to accommodate an additional misorientation due to the inclination of the vector. The magnitude of shear is estimated to be $|1/3[\bar{1}101]|\cdot\cos 84.16° = 0.052$ nm. This indicates that dislocations which have a component toward the $[\bar{2}20\bar{1}]$ direction should be periodically introduced to accommodate the shear due to the $1/3[\bar{1}101]$ component. Therefore, two or more kinds of perfect dislocations should be introduced, and thus the dislocation contrasts in Fig. 2 are not uniform. Also, dislocations which have the component along the $[\bar{2}20\bar{1}]$ direction should accompany asymmetric strain fields relative to the grain boundary plane, which forces the dislocations to move out of the boundary plane. This may be the reason why the dislocations are not arranged along a straight line, contrary to other low-angle grain boundaries in alumina [10–12, 14, 15].

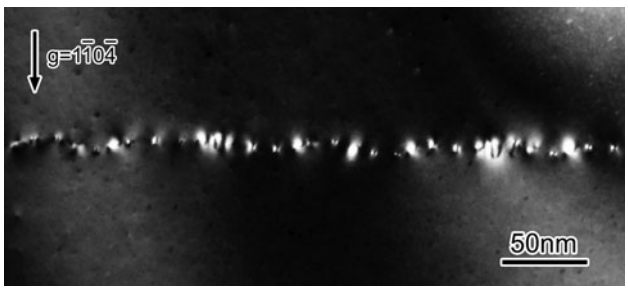

Fig. 3 A dark-field TEM image of the grain boundary obtained using the reflection $\boldsymbol{g} = (1\bar{1}0\bar{4})$. Small pair contrasts and relatively large contrasts can be seen along the grain boundary

Figure 4a is a high-resolution TEM image of dislocations in the boundary taken along the $[11\bar{2}0]$ zone axis. The right and the left dislocations are dissociated into two partial dislocations, while the center dislocation is of perfect type (undissociated). Figure 4b shows the core structure of the perfect dislocation. The Burger circuit indicates the edge components of the dislocation. It is found that the perfect dislocation has $\boldsymbol{b}_e = 1/2[\bar{1}100]$ edge component. This component can be represented as $1/6[\bar{1}101] + 1/6[\bar{2}20\bar{1}]$, which accommodates the mistilt and shear of the boundary. However, the component $\boldsymbol{b}_e = 1/2[\bar{1}100]$ does not correspond to a translation vector. Since the Burgers vector of a perfect dislocation must coincidence with a translation vector, a screw component along the $[11\bar{2}0]$ direction should be included in the perfect dislocation in Fig. 4b. Here, the screw component which generates the smallest translation vector is $\boldsymbol{b}_s = 1/6[11\bar{2}0]$ or $1/6[\bar{1}\bar{1}20]$, which are equivalent each other. Therefore, the Burgers vector of the perfect dislocation can be $\boldsymbol{b} = 1/3[\bar{1}2\bar{1}0]$ or $1/3[\bar{2}110]$ (i.e., $1/2[\bar{1}100] + 1/6[11\bar{2}0] \rightarrow 1/3[\bar{1}2\bar{1}0]$ or $1/2[\bar{1}100] + 1/6[\bar{1}\bar{1}20] \rightarrow 1/3[\bar{2}110]$).

The core structure of the dissociated dislocation pair is shown in Fig. 4c, with the partial dislocations split along the (0001) plane. This indicates that a stacking fault is formed on the (0001) plane in between the partial dislocations, and that the stacking fault on the (0001) plane may

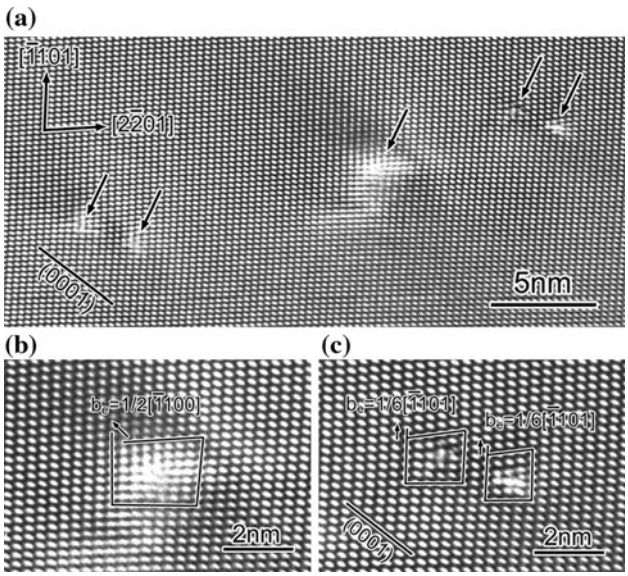

Fig. 4 **a** A high-resolution TEM image of the grain boundary. The center dislocation is not dissociated, while the right and the left dislocations are dissociated on the (0001) plane. **b** The enlarged image of the center dislocation in (**a**). The Burgers circuit indicates that the edge component of this dislocation is $1/2[\bar{1}100]$. **c** The enlarged image of the left dissociated-dislocation pair. Each dislocation has $1/6[\bar{1}101]$ edge component, and so the total edge component of dissociated-dislocation pair is $1/3[\bar{1}101]$

be relatively more stable than those of other possible planes, namely, the planes perpendicular to the $\{11\bar{2}0\}$ plane, such as $\{1\bar{1}00\}$, $\{1\bar{1}02\}$, and $\{\bar{1}104\}$. It is noted that the contrast of the stacking fault is similar to that of the bulk. The Burgers circuits indicate that each partial dislocation has an edge component of $\boldsymbol{b}_e = 1/6[\bar{1}101]$, and so the total edge component of the partial-dislocation pair is $\boldsymbol{b}_e^{tot} = 1/3[\bar{1}101]$, which mainly accommodates the mistilt of the boundary. Owing to the indefinite screw component, two possible total Burgers vectors of the partial-dislocation pair, $\boldsymbol{b}_1^{tot}$ and $\boldsymbol{b}_2^{tot}$, can be considered as follows. (1) Since the vector $1/3[\bar{1}101]$ corresponds to a translation vector, $\boldsymbol{b}_1^{tot} = 1/3[\bar{1}101]$ can be a Burgers vector of the perfect dislocation. (2) If the partial-dislocation pair has a screw component of $1/3[11\bar{2}0]$, $\boldsymbol{b}_2^{tot} = 1/3[02\bar{2}1]$ can be the second smallest Burgers vector of the perfect dislocation with $1/3[\bar{1}101]$ edge component (i.e., $1/3[\bar{1}101] + 1/3[11\bar{2}0] \rightarrow 1/3[02\bar{2}1]$). When the screw component is opposite in sign ($1/3[\bar{1}\bar{1}20]$), the total Burgers vector is $1/3[\bar{2}021]$, which is equivalent to the $1/3[02\bar{2}1]$ vector. Thus, it is enough to consider the two vectors of $\boldsymbol{b}_1^{tot}$ and $\boldsymbol{b}_2^{tot}$.

As mentioned above, each partial dislocation has the equivalent edge component of $1/6[\bar{1}101]$. The magnitude of the screw component of it is assumed to be zero or $|1/6[11\bar{2}0]|$ from the crystal structure. Other screw components (e.g.,: $1/9\langle 11\bar{2}0\rangle$) may be possible, but are too complex to be considered here. Thus, the following dissociation reactions can be considered for the perfect dislocations of $\boldsymbol{b}_1^{tot} = 1/3[\bar{1}101]$ and $\boldsymbol{b}_2^{tot} = 1/3[02\bar{2}1]$.

$$1/3[\bar{1}101] \rightarrow 1/6[\bar{1}101] + 1/6[\bar{1}101] \quad (2)$$

$$1/3[\bar{1}101] \rightarrow 1/6[02\bar{2}1] + 1/6[\bar{2}021] \quad (3)$$

$$1/3[02\bar{2}1] \rightarrow 1/6[02\bar{2}1] + 1/6[02\bar{2}1] \quad (4)$$

In the first case, the partial dislocations have no screw components. In the second case, they have antiparallel screw components of $1/6[11\bar{2}0]$ and $1/6[\bar{1}\bar{1}20]$. In the third case, they have equivalent screw components of $1/6[11\bar{2}0]$. The vector $1/6[\bar{1}101]$ does not correspond to a translation vector in either the cation or the anion sublattice, while the vector $1/6[02\bar{2}1]$ corresponds to a translation vector in the cation sublattice. Therefore, the dissociation of Eq. 2 generates a staking fault in both the anion and cation sublattices, and the dissociations of Eqs. 3 and 4 generate a staking fault in only the anion sublattice. Here, it was define stacking faults formed on the (0001) plane by the fault vectors $1/6[\bar{1}101]$ and $1/6[02\bar{2}1]$ as SF_{AC} and SF_A, respectively. The suffixes A and C mean the sublattice of anions and cations, respectively.

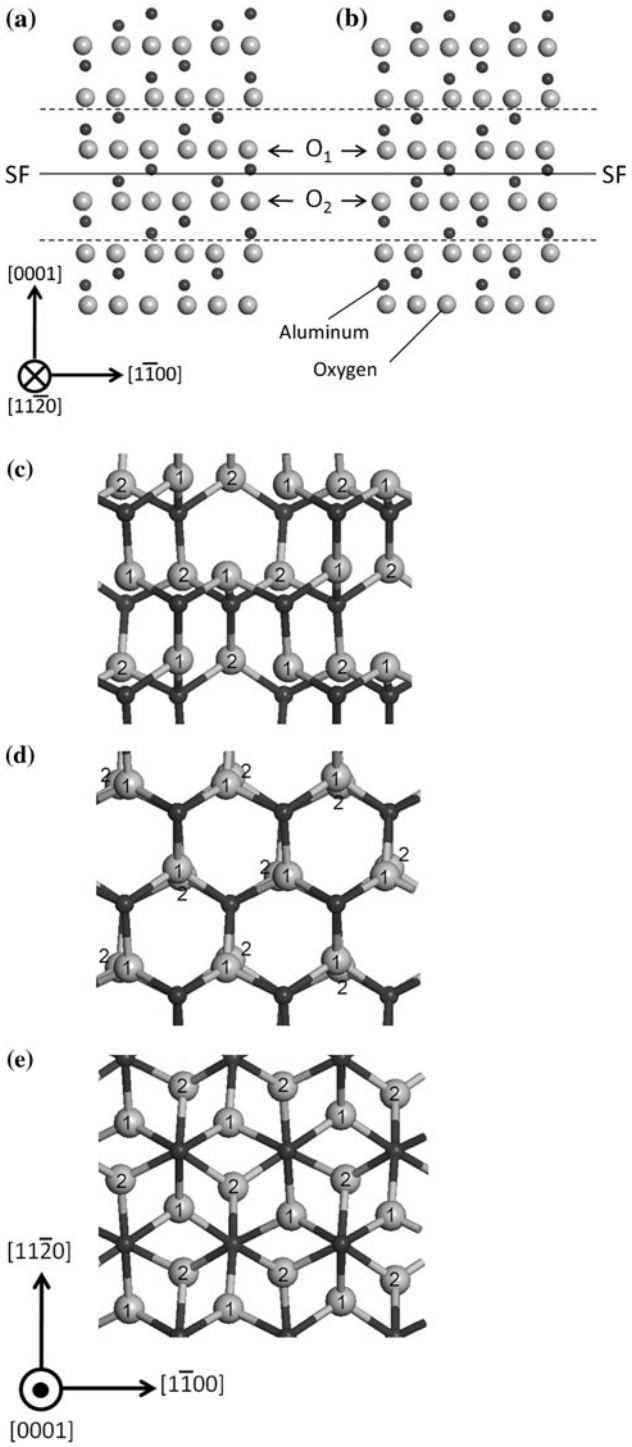

Fig. 5 Schematics showing the rigid models of SF_{AC} and SF_A. **a**, **b** show the $[11\bar{2}0]$ projection of SF_{AC} and SF_A, respectively. The positions of the stacking faults are indicted by the *solid line*; however, they cannot be confirmed in each model from this projection direction. **c**–**e** show the [0001] projection of SF_{AC}, SF_A, and the bulk, respectively. In these schematics the ions between the *broken lines* in (**a**) and (**b**) are described. The numbers *1* and *2* on the oxygen ions correspond to O_1 and O_2 in (**a**) and (**b**)

Figure 5a and b shows the rigid models of SF_{AC} and SF_A along the $[11\bar{2}0]$ projection, respectively. They are seen to have the same atomic configuration in this projection direction. The rigid model of SF_{AC} was constructed by removing 1/6[0001] thick of the (0001) plane and shearing the crystal by $1/6[\bar{1}100]$ on the (0001) plane. If the shear component is changed to $1/3[01\bar{1}0]$, SF_A is formed. The positions of the stacking faults are indicated by the solid line, but the atomic disorder of the stacking faults cannot be identified from the $[11\bar{2}0]$ projection. This is consistent with the fact that the high-resolution TEM contrasts of the stacking fault are bulk-like in Fig. 4. Figure 5c and d shows the [0001] projection of SF_{AC} and SF_A, respectively, over the five (0001) atomic layers between the broken lines in Fig. 5a and b. The atomic staking of the perfect crystal is shown in Fig. 5e. The oxygen ions notated by 1 and 2 are on different heights of (0001) planes, and correspond to atomic layers indicated by O_1 and O_2 in Figs. 5a and b. In the perfect crystal, the layers of O_1 and O_2 are arranged with a shift of $1/9[11\bar{2}0]$ with respect to each other, as seen in Fig. 5e. The shift of O_1 and O_2 in SF_{AC} is $1/6[1\bar{1}00]$, and the aluminum ions are also arranged by a shift of $1/6[1\bar{1}00]$ across the stacking fault. The layers of O_1 and O_2 in SF_A are overlapped with each other, and there is no stacking disorder in the cation sublattice.

Table 1 shows the lengths of the shortest O–Al bonds and the nearest O–O distance in the rigid model of SF_{AC}, SF_A, and the bulk. The first nearest O–Al bond in SF_{AC} is about 42% shorter than that in the bulk. This O–Al bond would be very unstable, and it may lead to quite high energy or the atomic positions may be considerably changed by relaxation. On the other hand, the length of the first nearest O–Al bond in SF_A is almost bulk-like, and the nearest O–O distance is about 12% shorter, which should increase electrostatic energy but not as much as in SF_{AC}. Also, the actual atomic configurations of the stacking fault may be close to the rigid models in Fig. 5, because the contrasts of high-resolution TEM of the stacking fault in Fig. 4 are similar to that of the bulk. The above considerations suggest that SF_{AC} would be more difficult to form than SF_A. Next, the authors discuss the staking fault energies based on the elastic theory.

Table 1 The lengths of the shortest O–Al bonds and the nearest O–O distance in the rigid model of SF_{AC}, SF_A, and the bulk

	O–Al (Å)	O–O (Å)
SF_{AC}	1.1	2.5
SF_A	1.9	2.2
Bulk	1.9	2.5

The elastic repulsive force between dislocations can be derived from the Peach–Koehler equation [22]. For a dissociated-dislocation pair, the excess energy of the stacking fault formed between them acts as attractive force. In the case that two dissociated dislocations are equivalent and parallel, this force balancing is finally described as follows;

$$\gamma = \frac{\mu}{2\pi}\left(\frac{b_e^2}{1-\nu} + b_s^2\right)\frac{1}{r}, \tag{5}$$

where γ is the stacking-fault energy, μ is shear modulus ($\sim$150 GPa) [23], ν is Poisson's ratio ($\sim$0.24) [24], and r is the separation distance between the partial dislocations. In Fig. 4a, the average separation distance between the partial-dislocation pairs is 2.6 nm. Assuming the dissociation reactions of Eqs. 2–4, the fault energies are estimated to be $\gamma_{AC} = 0.79\ Jm^{-2}$ for the dissociation reaction of Eq. 2, $\gamma_{A-1} = 0.27\ Jm^{-2}$ for Eq. 3 (in this case the sign before the term of b_s^2 in Eq. 5 is minus, because the screw components of the partials are antiparallel), and $\gamma_{A-2} = 1.3\ Jm^{-2}$ for Eq. 4. It is noted that these calculations do not take into account the contributions from other dislocations in the boundary.

In deformed alumina crystals, cation stacking faults on the $\{11\ \bar{2}\ 0\}$ or $\{1\bar{1}00\}$ planes are typically seen [1–3, 6, 7, 9–12, 14–16], while neither anion faults nor (0001) faults have been found. This implies that anion faults and (0001) faults have higher energies than such cation faults. Experimental values of cation fault energies are 0.2–0.3 Jm^{-2} for the $\{11\bar{2}0\}$ fault [9, 10, 16] and 0.4–0.5 Jm^{-2} for the $\{1\bar{1}00\}$ faults [15]. For (0001) cation faults, the fault energies were theoretically estimated to be 1.5–1.8 Jm^{-2} (depending on structure models) based on the local-density-functional theory [25]. Using these values as reference, it can be said that the value of γ_{AC} (=0.79 Jm^{-2}) appears to be too low, although SF_{AC} has O–Al bonds which are about 42% shorter than that of in the bulk. Thus, the dissociation reaction of Eq. 2 is energetically inconsistent. The value of γ_{A-1} (=0.27 Jm^{-2}) is rather low compared to the reference values, and so the dissociation reaction of Eq. 3 is also inconsistent. The value of γ_{A-2} (=1.3 Jm^{-2}) is lower to some extent than the theoretical fault energies of (0001) cation faults. Although the validity of the value is difficult to judge, it can be said that this value is not as unreasonable as the others, and thus that the dissociation reaction of Eq. 4 is the most probable of the three assumed reactions. Therefore, it is likely that the partial-dislocation pair in Fig. 4a corresponds to the dissociation reaction of Eq. 4 with SF_A.

The analysis suggests that the perfect and the partial dislocations in the $\{\bar{1}104\}/\langle 11\bar{2}0\rangle$ tilt grain boundary have screw components, while the total screw component of dislocations in a tilt boundary must be zero. Thus, the

screw components would alternate in sign. This is a possible configuration because, as mentioned earlier, the Burgers vectors of dislocations which have screw components toward the $[11\bar{2}0]$ and the $[\bar{1}\bar{1}20]$ directions are equivalent for the both cases of the perfect dislocation and the partial-dislocation pair. However, the configuration of the screw components is not elucidated by this study. There is also room to investigate dissociation reactions which the authors did not consider. In order to prove the dissociation reaction and the structure of the stacking fault on the (0001) plane, it is needed to identify the screw components of the dislocations by such as $\boldsymbol{g} \cdot \boldsymbol{b}$ analysis using conventional TEM.

Conclusion

Dislocation structures in a $\{\bar{1}104\}/\langle 11\bar{2}0\rangle$ 2° tilt grain boundary were investigated by high-resolution TEM. Based on the TEM observations and structural considerations, it was suggested that the grain boundary consists of $\boldsymbol{b} = 1/3\langle 02\bar{2}1\rangle$ dissociated-dislocation pairs and $\boldsymbol{b} = 1/3\langle \bar{1}2\bar{1}0\rangle$ perfect dislocations. Also, each dissociated-dislocation pair accompanied a stacking fault on the (0001) plane. It was consider that the dissociation reaction is likely to be $1/3\langle 02\bar{2}1\rangle \rightarrow 1/6\langle 02\bar{2}1\rangle + 1/6\langle 02\bar{2}1\rangle$, which generates a stacking fault in the anion sublattice. Assuming this dissociation reaction, the stacking fault energy was estimated to be roughly 1.3 Jm^{-2} based on the elastic theory.

Acknowledgements The authors would like to thank S.D. Findlay for critically reading the manuscript. This study was supported in part by the Grant-in-Aid for Scientific Research on Priority Areas "Nano Materials Science for Atomic-scale Modification" (no. 19053001) from the Ministry of Education, Culture, Sports and Technology (MEXT). E.T. was supported as a Japan Society for the Promotion of Science (JSPS) research fellow. N.S. acknowledges supports from PRESTO, Japan Science and Technology Agency, and the Grant-in-Aid for Young Scientists (A) (20686042) from MEXT.

References

1. Mitchell TE, Pletka BJ, Phillips DS, Heuer AH (1976) Philos Mag 34:441
2. Bilde-Sørensen JB, Tholen AR, Gooch DJ, Groves GW (1976) Philos Mag 33:877
3. Phillips DS, Mitchell TE, Heuer AH (1982) Philos Mag A 45:371
4. Phillips DS, Pletka BJ, Heuer AH, Mitchell TE (1982) Acta Metall 30:491
5. Cadoz J, Castaing J, Phillips DS, Heuer AH, Mitchell TE (1982) Acta Metall 30:2205
6. Lagerlöf KPD, Mitchell TE, Heuer AH, Riviere JP, Cadoz J, Castaing J, Phillips DS (1984) Acta Metall 32:97
7. Lagerlöf KPD, Heuer AH, Castaing J, Riviere JP, Mitchell TE (1994) J Am Ceram Soc 77:385
8. Inkson BJ (2000) Acta Mater 48:1883
9. Nakamura A, Yamamoto T, Ikuhara Y (2002) Acta Mater 50:101
10. Ikuhara Y, Nishimura H, Nakamura A, Matsunaga K, Yamamoto T, Lagerlöf KPD (2003) J Am Ceram Soc 86:595
11. Nakamura A, Matsunaga K, Yamamoto T, Ikuhara Y (2006) Philos Mag 86:4657
12. Shibata N, Chisholm MF, Nakamura A, Pennycook SJ, Yamamoto T, Ikuhara Y (2007) Science 316:82
13. Lartigue-Korinek S, Liagege S, Kisielowski C, Serra A (2008) Philos Mag 88:1569
14. Tochigi E, Shibata N, Nakamura A, Yamamoto T, Ikuhara Y (2008) Acta Mater 56:2015
15. Tochigi E, Shibata N, Nakamura A, Mizoguchi T, Yamamoto T, Ikuhara Y (2010) Acta Mater 58:208
16. Heuer AH, Jia CL, Lagerlöf KPD (2010) Science 330:1227
17. Choi S-Y, Buban JP, Nishi M, Kageyama H, Shibata N, Yamamoto T, Kang S-JL, Ikuhara Y (2006) J Mater Sci 41:2621. doi:10.1007/s10853-006-7824-9
18. Igarashi M, Sato Y, Shibata N, Yamamoto T, Ikuhara Y (2006) J Mater Sci 41:5146. doi:10.1007/s10853-006-0447-3
19. Read WT, Shockley W (1950) Phys Rev 78:275
20. Frank FC (1951) Philos Mag 7th Ser 42:331
21. Lee WE, Lagerlof KPD (1985) J Electron Microsc Tech 2:247
22. Hirth JP, Lothe J (1982) Theory of dislocations, 2nd edn. Krieger Publishing Company, Malabar
23. Chung DH, Simmons G (1968) J Appl Phys 39:5316
24. Gieske JH, Barsch GR (1968) Phys Status Solidi 29:121
25. Marinopoulos AG, Elsässer C (2001) Philos Mag Lett 81:329